ACS APPLIED MATERIALS & INTERFACES

www.acsami.org

Research Article

Combining CRISPR-Cas12a with Microsphere Array-Enhanced Fluorescence for Portable Pathogen Nucleic Acid Detection

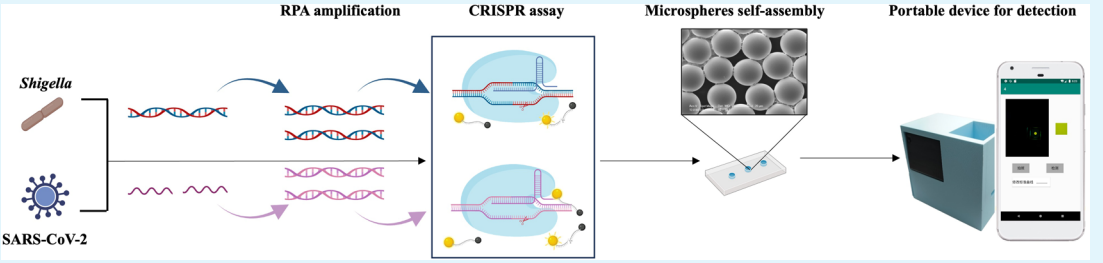
Menglu Gao,[⊥] Chen Yang,[⊥] Wu Si,[⊥] Xiaodan Xi,[⊥] Liangjun Chen, Zhikun Zeng, Yuan Rong,* Yi Yang,* Fubing Wang,* and Chunhui Yuan*

Cite This: https://doi.org/10.1021/acsami.5c00655

Read Online

ACCESS | Metrics & More | Article Recommendations | Supporting Information

Downloaded via SHANGHAI NORMAL UNIV on March 29, 2025 at 01:28:11 (UTC).
See https://pubs.acs.org/sharingguidelines for options on how to legitimately share published articles.



ABSTRACT: The detection of food contamination in a swift and sensitive manner is essential for safeguarding public health. Clustered regularly interspaced short palindromic repeats (CRISPR)-based assays for nucleic acid detection are renowned for their high specificity and convenient, related studies have focused on refining the Cas protein and optimizing the CRISPR (cr)RNAs design within CRISPR-based assays for enhancing the sensitivity of nucleic acid detection. Our research offers innovative insights into enhancing the fluorescence signal output intensity from a physical standpoint, thereby presenting a practical and cost-effective strategy to lower the detection thresholds in CRISPR-based assays. By a layer of microsphere arrays was spread onto the bottom of the microfluidic chip to enhance the fluorescence signal of the sample via self-assembly of the microspheres. Recombinase polymerase amplification (RPA) was used to amplify target sequences, followed by crRNA binding to activate Cas enzyme, cleaving fluorescein amidite (FAM)-labeled reporters and emitting a fluorescent signal. The method successfully identified SARS-CoV-2 positive samples (10 clinical samples and 8 environmental contamination samples) and distinguished them from negative samples. Meanwhile, it successfully detected 4 food contamination *Shigella* samples and 5 clinical *Shigella* samples. In this study, the developed method exhibited a detection limit (LoD) of 75 fM for SARS-CoV-2 (POCT with USB camera: 50 fM) and 100 fM for *Shigella* (POCT with USB camera: 75 fM). It also demonstrated promising sensitivity (100%) and specificity (100%) in a small-sample validation. Combined portable and automated detection was achieved using a smartphone to receive and process the fluorescent signals obtained from the samples. The detection platform developed in this study is not only applicable for the detection of pathogens in cold-chain food products, but also extends to pathogen detection in community hospitals and resource-limited areas, providing an efficient solution for rapid pathogen screening in different settings. Moreover, different nucleic acid samples can be detected by changing the RPA primer and CRISPR crRNA. This method provides a paradigm for studying enhanced fluorescence signaling and holds significant potential to advance the commercialization and practical use of CRISPR fluorescence sensors.

KEYWORDS: *nucleic acid detection, microspheres, fluorescence enhancement, CRISPR, pathogen detection*

1. INTRODUCTION

Regarding food safety, cold chains play a pivotal role in maintaining the integrity of perishable goods; however, it is essential to recognize that controlled low temperatures, which are critical for preserving food quality, may also create an environment conducive to the survival of certain foodborne pathogens. *Shigella*, a prominent foodborne pathogen, poses a significant health risk, with the ability to spread through food contamination and induce diseases in humans.[1,2] Concurrently, studies have shown instances where the novel coronavirus, known primarily for its respiratory transmission, has potentially been disseminated via cold chain food products. This mode of transmission is of particular concern because of the virus's capacity to survive in low-temperature environments typical of cold chain logistics, raising the possibility of cold chain food acting as a conduit for the spread of COVID-19.[3,4] Therefore, as critical measures in controlling the spread of infectious diseases, timely and precise pathogen detection is essential for

Received: January 13, 2025
Revised: March 22, 2025
Accepted: March 23, 2025

© XXXX American Chemical Society

effectively managing the source of infection and promptly severing the transmission pathways.

Nucleic acid testing is a common method for detecting viruses and bacteria. Conventional nucleic acid assays typically use the PCR, proven to have high accuracy and sensitivity.[5−8] However, this technique usually requires complex equipment and specialized operators, is time-consuming, and can usually only be performed in the laboratory, severely limiting its application and development in the field of point-of-care testing (POCT). Nucleic acid detection based on CRISPR technology is a novel and highly efficient nucleic acid detection method that utilizes the specific recognition and cleavage ability of the CRISPR-Cas system to achieve the rapid and sensitive detection of target deoxyribonucleic acid (DNA) or ribonucleic acid (RNA) sequences.[9−13] This technology eliminates the temperature cycling process required for PCR, which greatly reduces the reaction time, and is easy to operate by simply mixing the sample to be tested with the probe solution. Combined with a portable signal-reading device, it enables nucleic acid detection anywhere and anytime. Nucleic acid detection based on CRISPR technology usually requires analysis of the fluorescence signal of the sample. Conventional devices for detecting fluorescence signals are bulky, inconvenient to operate, and unsuitable for POCT. The use of smartphones to detect nucleic acids in samples has been reported.[14−17] To ensure portability of the devices, the amount of sample used in a single assay was small; therefore, the resultant fluorescence signal was weak, leading to a high detection limit for these devices. Therefore, there is a requirement for more sensitive methods of portable nucleic acid detection devices using smartphones.

Microfluidics and "lab-on-a-chip" enable flexible biochemical sample manipulation and on-chip integration of multiple technologies.[18−22] Different chip structures can be designed based on optofluidics, and optofluidic sensors with excellent performance can be fabricated.[23−25] At present, optofluidic microarrays have been applied in biological detection. Studies have been reported on POCT devices that can detect a variety of biomarkers and viruses[26,27] In addition to the "multiplexed digital ELISA" technology that can detect a variety of biomarkers in a continuous and rapid manner.[28] Optofluidic technology combined with smartphones can enable the real-time rapid detection of weak optical signals. Utilizing the focusing and optical microcavity effects of the microsphere system enhances the fluorescence signal of the sample and improves detection sensitivity.[22,29−31]

This study presents a method for the portable and accurate quantitative detection of nucleic acids in combination with a smartphone utilizing optical microcavities to enhance the fluorescence signal Within the realm of molecular diagnostics, the combination of CRISPR and RPA technologies offers a robust platform for the rapid and specific detection of nucleic acids at ambient temperatures. The straightforward design of a microsphere array enhances the sensitivity of CRISPR-based detection, enabling it for swift and precise identification of food contamination. This paper aims to rapidly and sensitively detect cool chains foodborne pathogens, specifically *Shigella* and SARS-CoV-2, utilizing the aforementioned strategies.

2. MATERIALS AND METHODS

2.1. Materials. The PDMS chip, a microfluidic chip made from polydimethylsiloxane, was purchased from Dow Corning (NY). SU8 2100 adhesive was purchased from MicroChem (Dalian, China). The polystyrene (PS) microspheres were purchased from Beijing Zhongkeleiming Daojin Technology. Rhodamine 6G (R6G) and fluorescein isothiocyanate (FITC) were purchased from Merck. Cyanine5 (Cy5) was purchased from DuoFluor (Wuhan, China).

2.2. Fabrication of the Microsphere Microfluidic Chip. The PDMS chip was fabricated using the traditional method. The AB adhesive was mixed in accordance with the mass ratio of 10:1 and used to cover the silicon plate (substrate), followed by heating in an oven at 75 °C for 1 h. The solidified PDMS material was then peeled off from the silicon plate and cut into small square pieces approximately 2 cm × 2 cm. Punch a hole in the PDMS using a 3 mm diameter metal hole punch. After oxygen plasma treatment, the channel was sealed on a 3 × 3 cm^2 glass. Next, 2 μL of PS microspheres with a concentration of 10 mg/mL and a diameter of 8 μm was dropped on the bottom of the channel and then placed in a ventilated area to obtain a layer of PS microspheres on the bottom of the channel once the liquid has evaporated. The microsphere system was located on a glass backing plate in the middle of the microfluidic chip at the vacant position.

2.3. System Design. The system contained a replaceable nucleic acid detection chip, a power supply module, and a fluorescence system using a smartphone as the receiver for the fluorescence signal. The power supply system required a 12 V battery as the power source. The fluorescence system consisted of a small laser and its cooling unit (Daheng Optics), a bandwidth laser reflector (400−700 nm, Daheng Optics), and two bandpass filters (Daheng Optics). The laser and first filter wavelengths were the excitation wavelengths of the sample, and the second filter wavelength was the emission wavelength of the sample. The first filter is used to filter the stray light produced by the phenomena of reflection and refraction of the laser in the device and the second filter is used to filter the excitation light. The laser light passed through the reflector and was incident vertically on the first filter. The excitation light passed through the first filter and entered the sample inside the microfluidic chip, where the sample was excited, generating a fluorescent signal. The fluorescence produced by the sample was captured using a smartphone. The image was analyzed using the developed algorithms, and the results were displayed on the user's smartphone interface. The overall size of the device and detection area were designed with a light shield to isolate the chip from the outside environment. The device weighed <1 kg.

Considering that different smartphone cameras have different parameters and some of them may not be able to fit completely into the shooting hole when taking pictures, which may result in light leakage and affect the test results, as shown in Figure S1, we have additionally developed a portable testing device that uses an internal integrated USB camera to avoid these problems, which may not be as good as a smartphone camera in terms of image quality (pixel value, etc.). USB cameras may not have the same image quality (pixel value, etc.) as smartphone cameras, so users can choose the appropriate device for sample testing according to their needs.

2.4. Nucleic Acid Detection Using a Microcavity-integrated Platform. A total of 10 μL of the sample was added to the microfluidic chip, which was placed into the device with the detection area aligned to where the excitation light passes through. The front of the cassette was covered to minimize external light interference. Then, the laser battery box was turned on, and after observing the stable fluorescence signal at the upper shooting window, the smartphone camera was placed at the shooting window. The camera was turned on and adjusted to professional mode, and the ISO parameter was set to 200 and the shutter time (S) to 1/50 s. The camera was focused on the fluorescence signal in the detection chamber, and a picture was taken. The application was opened, the captured image was selected, and the analyze button was clicked to obtain the sample concentration.

2.5. Image Processing and Detection. After selecting an image, it was first filtered for stray light. The image pixels were checked individually, and the brightness (V value) of the pixels with the H value in a specific range (not the range of the filter used in front of the lens) was modified to zero, which is black. The brightest region of the image (200 × 200 pixels) was obtained. First, we made a brief

https://doi.org/10.1021/acsami.5c00655
ACS Appl. Mater. Interfaces XXXX, XXX, XXX−XXX

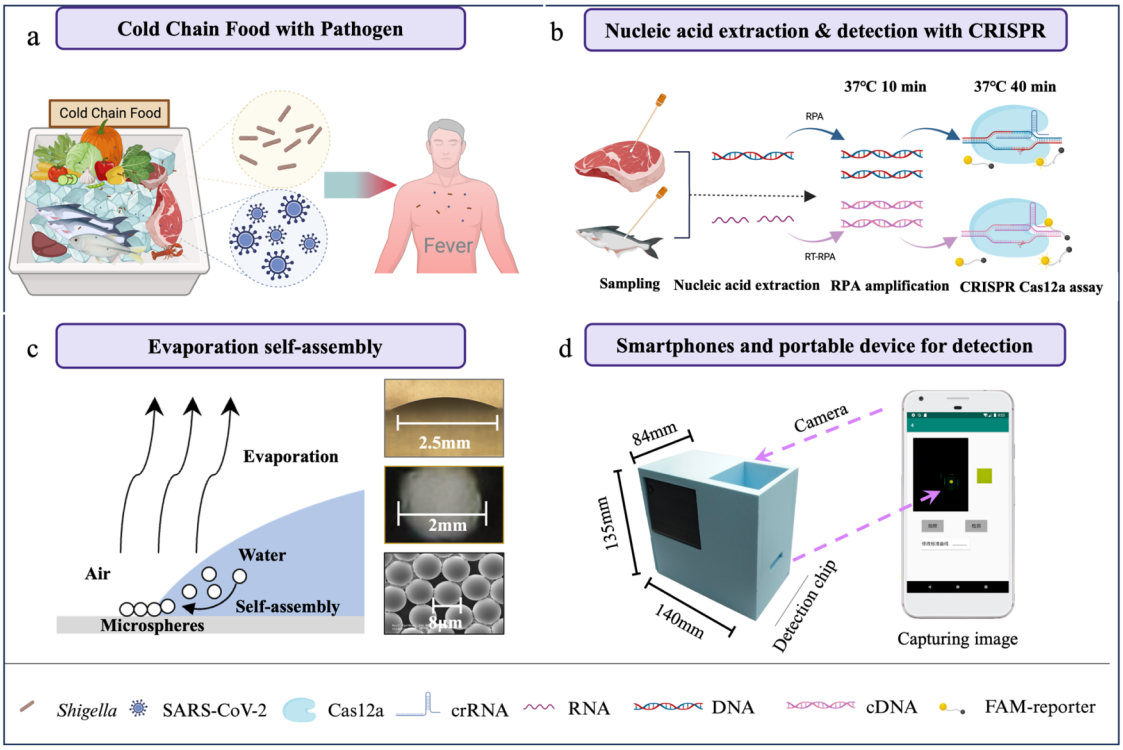


Figure 1. Schematic illustration of the RPA-CRISPR-based pathogen detection in cold chain food and the portable device. (a) Pathogens carried by cold-chain food can cause diseases in humans. (b) Workflow of RPA and CRISPR-based pathogen detection in cold chain food: RPA/RT-RPA at 37 °C for 10 min, followed by a CRISPR reaction at 37 °C for 40 min (c) Microsphere system for signal enhancement through evaporation self-assembly. (d) The portable device and smartphone used for signal acquisition and analysis.

judgment to avoid too many calculations. The judgment condition was that the sum of the V value of a pixel and the pixel 10 pixels away from the pixel above (y + 10), the pixel 10 pixels away from the pixel below (y − 10), the pixel 10 pixels away from the pixel on the left side (x − 10), and the pixel 10 pixels away from the pixel on the right side (x + 10) was ≥50. When a pixel satisfied the above conditions, the calculation was based on its brightness (V). The sum of the V values of 121 pixels in a circular area centered on it, with a radius of 25 pixels and a step of 5 pixels, that is, the VA value, was then calculated. The VA values of all the pixels that satisfy condition one were calculated, and the maximum value was selected. Taking the pixel point with the largest VA value as the center, an area of 200 × 200 pixels was intercepted, which was the brightest area. The image of the brightest region was then segmented into three single-channel images, R, G, and B. The average pixel values of the three images were weighted according to the wavelength of the signal from the fluorescent solution (532 nm) and the wavelength of the excitation light (488 nm) and merged into a single-channel image. Since the fluorescent signal is green light at 532 nm and the excitation light is cyan-blue light at 488 nm, three single-channel images were synthesized using $N = 0.9*R + 0.0*G + 0.1*B$, and N is the pixel value of the synthesized image. The synthesized single-channel images were then Fourier transformed and the homomorphic filter (see Supporting Information for specific parameters) was used to process the transformed images, after which the processed images were inverted to obtain the enhanced images. The pixel values of the enhanced image are brought into the standard curve to obtain the detection results.

2.6. Cas-Related Materials Methodology. *2.6.1. Construction and Amplification of Reference Plasmids.* Reference plasmids were generated through a cloning process in which the *N* gene sequence of SARS-CoV-2 (NC_045512) and the *hypothetical protein* (accession: AE014073, region: 4170556−4171068) of *Shigella* were individually inserted into the pUC57 vector. Reference plasmids were synthesized by GenScript Biotech (Shanghai, China). The recombinant plasmids were then introduced into DH5*α E. coli* strains. An initial inoculation was performed on Luria−Bertani (LB) agar containing 50 μg/mL ampicillin to ensure resistance. This was followed by an overnight incubation at 37 °C for 20 h. Subsequently, monoclonal colonies were selected from the agar and transferred to a liquid LB medium supplemented with 50 μg/mL ampicillin. This culture was then incubated at 37 °C with a shaking speed of 200 rpm for an additional 12 h. After amplification, the plasmids were extracted and purified using an Endo Free Plasmid Kit (CwBio Biotech, China). These purified recombinant plasmids served as positive controls for assessing the performance of the CRISPR-RPA assay.

2.6.2. RPA Primer and crRNA Sequences. The CRISPR (cr)RNA and RPA primers designed to target the *N* gene of SARS-CoV-2 were derived from Chiu et al.[32] Additionally, primers targeting the highly conserved *hypothetical protein* gene of *Shigella* were supplied by Li et al.[33] A comprehensive list of all crRNA and RPA primer sequences utilized in this study can be found in Supplementary Table S1. The fluorescent-labeled DNA reporters used to signify the trans-cleavage signal of the CRISPR/Cas12a system were the FAM-TTATT-BHQ1 (F-Q) reporters. All primers, reporters, and crRNAs were synthesized by GenScript Biotech.

2.6.3. Preparation of the Pathogen Samples. The test samples in this study include clinically acquired samples, environmental contamination samples, and food contamination samples. All samples used in this study were collected under the auspices of the Ethics Committee at Zhongnan Hospital, with approval ID KL 2021024, and were in strict accordance with the ethical principles of the Declaration of Helsinki. Nucleic acid extraction was performed according to the protocol specified by the manufacturer (Takara No9766, Japan). The extracted nucleic acids were stored at −80 °C for future analyses.

2.6.4. RPA/RT-RPA and CRISPR Assay. To prepare the RPA reagent from its lyophilized form, 29.5 μL of rehydration buffer was added to the powder and thoroughly mixed. Then, 2.4 μL of each 10 μM forward and reverse primer, 10.2 μL of nuclease-free water, and 3 μL of the target nucleic acid or recombinant plasmid was added to the mixture. In the reverse transcriptase (RT)-RPA assay, 0.5 μL RT (200 U/μL, Toyobo, Japan) was added separately. The amplification phase

https://doi.org/10.1021/acsami.5c00655
ACS Appl. Mater. Interfaces XXXX, XXX, XXX−XXX

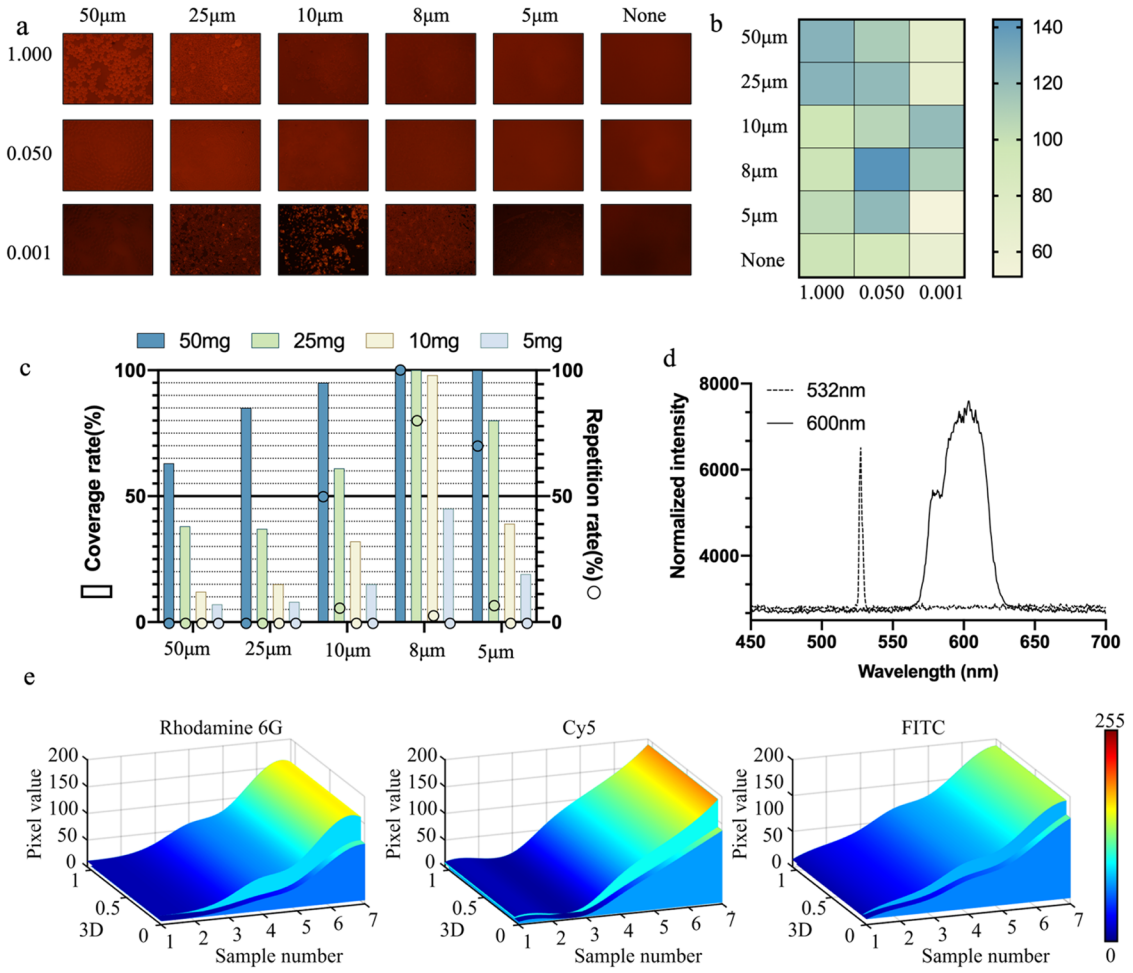


Figure 2. Schematic diagram of fluorescence signal enhancement effect of microspheres of different sizes on different concentrations of fluorescent solutions. (a) and (b) Fluorescence enhancement effect of microspheres of different sizes on rhodamine 6G solution (1.000 g/L, 0.050 g/L, 0.001 g/L). (c) Self-assembly effect of microspheres of different sizes and concentrations. (d) Wavelength diagram of excitation light and signal receiving module filter. (e) Fluorescence signal enhancement effect of 8 μm microspheres on rhodamine 6G, FITC, and Cy5 solutions.

using RPA primers to target the sequence of interest was performed at 37 °C for 10 min.

The amplified products could be stored at −20 °C for future applications or used immediately in the subsequent CRISPR reaction. The CRISPR reaction included 3 μL of 1 × NEB buffer 2.1, 30 nM of crRNA, 30 nM of LbcCas12a, 500 nM of the F-Q ssDNA reporters, and 3 μL of the amplified products, with nuclease-free water to adjust the volume to exactly 30 μL. Complete mixing of the components was ensured, followed by incubation at 37 °C for 40 min. Fluorescence signals were assessed (Bio-Rad, CFX96).

2.6.5. RT-qPCR. Prior to testing, nucleic acid extraction is carried out on the samples. *Shigella*'s nucleic acid is extracted utilizing the Shenggong bacterial DNA kit, while the RNA of the novel coronavirus is isolated with the Takara virus RNA kit. Subsequently, the RNA undergoes reverse transcription to cDNA, a process facilitated by a kit also sourced from Takara. The qPCR mix consists of 1X Goldstar probe mix, 2 μL template DNA, 0.2 μM probe, 0.2 μM each of forward and reverse primers, and ultrapure water to a final volume of 50 μL. The qPCR protocol is 10 min at 95 °C, followed by 30 cycles of 15 s at 95 °C and 60 s at 60 °C. Fluorescence is measured using the Bio-Rad CFX96 (USA).

2.6.6. Software. Figures 1a,b and and 4a were created using BioRender, with permission (Agreement number: VQ27DR4ATX). Data were analyzed through GraphPad Prism 10.0.

3. RESULTS AND DISCUSSION

3.1. Overview of the Microsphere-Based CRISPR Platform. Cold chain food carriers have the potential to carry harmful pathogens, including SARS-CoV-2 and *Shigella*, which can lead to infections and trigger various diseases in humans, as depicted in Figure 1a. The microsphere-based CRISPR platform developed in this study was specifically designed to detect pathogenic nucleic acids in cold chain foods, offering a reliable method for ensuring food safety and public health. After collecting pathogen samples and extracting nucleic acids, nucleic acid amplification is performed using RPA/*RT*-RPA at 37 °C for 10 min, followed by a CRISPR reaction at 37 °C for 40 min to cleave the FAM reporter and generate fluorescence (Figure 1b). The microsphere system shown in Figure 1c enhances the fluorescence signal for sample detection. Using the portable device and smartphone shown in Figure 1d for signal acquisition and analysis, rapid, accurate, and portable nucleic acid detection of pathogens in samples can be achieved.

3.2. Construction of Microsphere Systems. During the evaporation of the microsphere solution, the microspheres in the solution spontaneously and regularly arranged, and the concentration of the microspheres affected the final arrangement. When the density of the ultimately formed microsphere

https://doi.org/10.1021/acsami.5c00655
ACS Appl. Mater. Interfaces XXXX, XXX, XXX−XXX

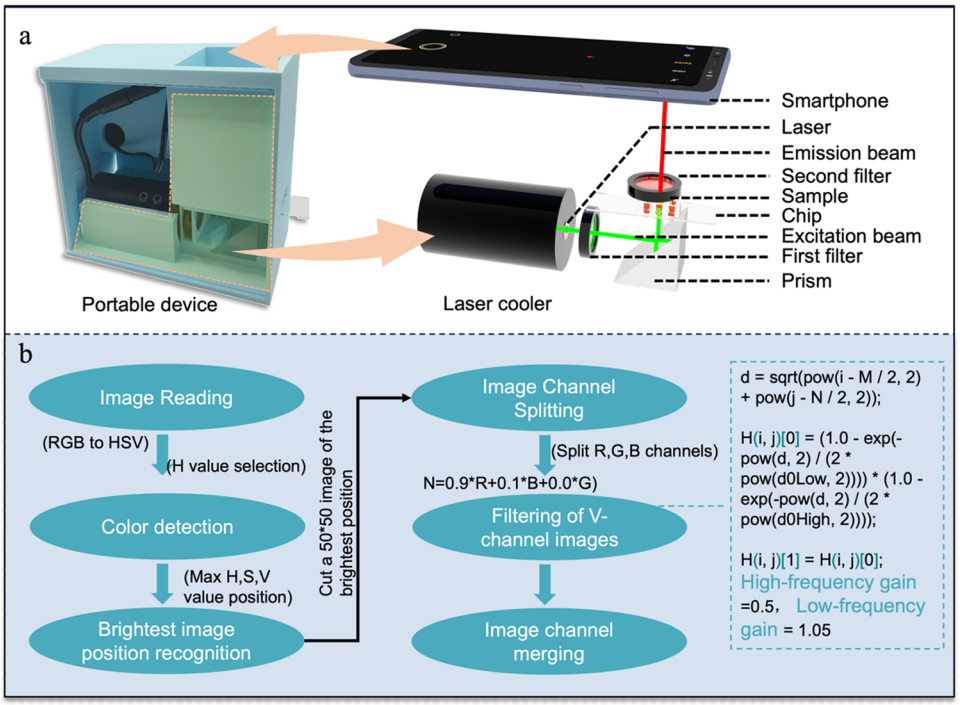


Figure 3. Structure and working principle of the portable device. (a) Portable device and optical path and (b) image processing process and algorithm.

system is low and it is not possible to cover the bottom of the detection area in the form of a single layer of microspheres, the area not covered by a single microsphere does not have a fluorescence enhancement effect, and therefore its fluorescence signal is weak. And when the density of the final formed microsphere system is high, overlapping of multilayer microspheres will occur in some areas. When multiple microspheres are overlapped, the fluorescent solution is difficult to enter the middle of the multilayer microspheres due to the fact that the microsphere material is polystyrene (PS), which is hydrophobic, resulting in almost no fluorescence signals on the overlapped part. Therefore, the microsphere system has the best fluorescence signal enhancement effect when it completely covers the bottom of the detection area in the form of a single layer of microspheres. To investigate the effect of microsphere concentration on the self-assembly effect, self-assembly experiments were performed on glass slides using different concentrations of microspheres in a volume of 2 μL. This self-assembly effect is illustrated in Figures 1a and S2. When the concentration was high, two or more layers of microspheres formed at the bottom of the chip, whereas the lower concentration failed to spread well to the bottom of the chip. The fill rate indicates the area ratio occupied by the microsphere system in the self-assembly region, and the coverage rate indicates the area ratio occupied by two or more stacked microsphere regions in the self-assembly region. As shown in Figure 2c, when the 50 μm microsphere has a concentration of 50 mg/mL, 25 μm of 50 mg/mL, 10 μm of 25 mg/mL, 8 μm of 10 mg/mL, and 5 μm of 10 mg/mL, the microsphere system can be formed with a high coverage and a low repetition rate.

3.3. Effect of Microsphere Size on Fluorescence Signal Enhancement. The fluorescence enhancement mechanism of microsphere arrays has two main aspects one is the spherical resonator effect. Since the refractive index of microspheres (n_{MS} = 1.6) is larger than that of the surrounding liquid (n_L = 1.332), each microsphere can be regarded as a spherical resonator, thus enhancing the fluorescence signal on the surface of the microspheres.[27−29] The second is the focusing effect of microspheres, the high refractive index of microspheres makes each microsphere can be regarded as a convex lens, the excitation light and the fluorescence signal generated by the solution at the bottom of the microsphere passes through the microsphere and then converge at the focal point not far away from the surface of the microsphere, which enhances the fluorescence signal on the surface of the microsphere.[30] Although theoretically calculating the specific enhancement effect of the microsphere system is still a difficulty faced at present, however, a clear fluorescence enhancement.

Since the quality factor of each microsphere when acting as a spherical resonator is affected by the size of the microsphere, its fluorescence enhancement effect varies with the size of the microsphere. Therefore, it is necessary to select microspheres of appropriate sizes to construct the microsphere system.

To verify the enhancement effect of microspheres with different diameters on the fluorescence signals, fluorescence signal enhancement experiments were performed using microspheres with diameters of 50, 25, 10, 8, and 5 μm against R6G solutions with concentrations of 1, 0.05, and 10^{-3} g/L, respectively. The fluorescence signals of the samples were read using an inverted fluorescence microscope with a volume of 10 μL of fluorescent solution for each concentration. The microsphere system was constructed using a microsphere concentration of 2 μL close to a full layer of microspheres. The results of these experiments are shown in Figure 2a,b. It can be seen that 50 and 25 μm microspheres could enhance the fluorescence signal of the higher concentration (1 g/L) R6G solution but could not enhance the fluorescence signal of the lower concentration (10^{-3} g/L) R6G solution. The 10 and 8

https://doi.org/10.1021/acsami.5c00655
ACS Appl. Mater. Interfaces XXXX, XXX, XXX−XXX

μm microspheres could not enhance the fluorescence signal of the higher concentration R6G solution but could enhance the fluorescence signal of the lower concentration R6G solution. The 5 μm microspheres did not enhance the fluorescence signal of both the high and low concentration R6G solution. In practice, the fluorescence signal of lower concentration nucleic acid samples tends to be weaker, thus, 8 μm microspheres were chosen to construct the microsphere system. To verify the enhancement effect of multilayer microspheres on the fluorescence signals of the samples, the fluorescence signal enhancement experiments were performed on R6G solution with a concentration of 10^{-4} g/L using 8 μm microspheres with concentrations of 25, 10, 5, and 2.5 mg/mL, respectively. The experimental results are shown in Figure S3, which indicates that a single layer of microspheres can significantly enhance the fluorescence signal of the solution while the enhancement effect of two or more layers of microspheres is weakened. When the microsphere concentration was greater than 10 mg/L, the microsphere system had no fluorescence signal enhancement effect on the fluorescent solution. And the microsphere systems constructed with different concentrations of microsphere solutions did not observe fluorescence signals in the control group (deionized water), indicating that they do not enhance the background noise. Therefore, the microsphere solution (10 mg/L) that can form a single-layer microsphere system was chosen to construct a microsphere system with a diameter of 8 μm.

In order to verify the stability of the microsphere system, we constructed three groups of microsphere systems using 8 μm microsphere solution with a concentration of 10 mg/L and performed stability and reproducibility tests, and the results of the stability experiments are shown in Figure S4, It can be seen that only a small portion of the constructed microsphere system will diffuse into the solution after adding fluorescent solution for 1h, and the rest of the microspheres can still maintain their original shapes very well, which shows that the microsphere system has good stability. The results of the reproducibility experiments are shown in Figure S5, which shows that the three groups of microsphere systems have almost no difference in shape and size, and their fluorescence enhancement effects on FAM solution also have no obvious difference, which surfaces that they have a good reproducibility in terms of shape and fluorescence enhancement effects.

3.4. Fluorescence Signal Enhancement Algorithm Based on Homomorphic Filtering. Relevant experiments were conducted to verify the enhancement effect of the image enhancement algorithm based on homomorphic filtering, and the specific parameters of the homomorphic filter are shown in the Supporting Information. The equation for the distance from each point to the center (crow, ccol) in the frequency domain is shown in eq (1). The filter function is shown in eq (2). Figure 3a shows the steps of image enhancement: first, the RGB channels of the image are divided into three single-channel images, and then the three mono images are combined into one single-channel image according to a certain ratio based on the image color. In this experiment, cyan-blue light with a wavelength of 488 nm was used as the excitation light, while the fluorescence signal emitted by the sample was green light with a wavelength of 532 nm, and thus the captured fluorescence image had a high average G value, a low R value, and an almost zero B value. Therefore, the weights of $N = 0.9*R + 0.1*G + 0.0*B$ were chosen. The merged images were then Fourier transformed and processed with a homomorphic filter, and then the images were inverted to obtain enhanced images. The fluorescence images before and after enhancement of the positive sample (deionized water) and the negative sample (10^{-1} g/L FAM solution) are shown in Figure S6, and the pixel values are shown in Figure S7, from which it can be seen that the signal value of the blank sample before and after enhancement of the image was enhanced from 5.01 to 5.246, which is an enhancement of 4.71%, and that the signal value of the positive sample before and after enhancement of the image was changed from 165.15 to 213.02, which is enhanced by 28.99%, so the signal-to-noise ratio changes from 40.61 to 32.96, which is a significant increase in signal-to-noise ratio.

3.5. The Structure and Working Principle of the Portable Device. Figure 3a displays the inner components of the compactly engineered portable device, characterized by its miniature dimensions ($14 \times 8.4 \times 13.5$ cm^3), lightweight (<1 kg), and uncomplicated design, enhancing its portability. The microsphere system utilizes the focusing effect and microcavity effect to enhance the fluorescence signal of the sample, which improves the LoD and sensitivity of the portable device. Figure 3b outlines the detection analysis procedure, with the capability to deliver test outcomes directly to a smartphone (Figure S9). The color filtering and localization algorithms in the image processing process can reduce the influence of background noise, obtain the most effective fluorescence signal, and improve the signal-to-noise ratio. The subsequent Fourier transform and homomorphic filtering process can enhance the fluorescence image to further improve the LoD and sensitivity. The parameters of the homomorphic filter are shown in Figure 3. Such a design enhances the applicability of CRISPR technology for diagnostic purposes in areas with limited resources.

3.6. Fluorescent Solution Test Results for Portable Devices. In our quest to find the most effective wavelengths, we evaluated the best-suited filters for R6G, FITC, and Cy5 individually. As shown in Figure 2d, the spectral distribution of the laser passing through the 532 nm filter shows that the excitation light passing through the filter has a good monochromaticity. Figure 2d also shows the spectrum of the white light source through the 600 nm filter, which can receive a larger wavelength range of light, while the excitation light cannot pass through the filter. The transmittance spectra of the filters of Groups B and C are shown in Figure S8.

To verify the fluorescence detection effect of the portable device, fluorescence detection was performed on different concentrations of R6G, FITC, and Cy5 fluorescent solutions using a chip with microspheres and a chip without microspheres, with deionized water as the solvent. Three groups of experiments were performed. Group A was the R6G solution with concentrations of 0, 10^{-3}, 10^{-4}, 10^{-5}, 10^{-6}, 10^{-7}, and 10^{-8} g/L respectively. The two filters were centered at 532 and 600 nm, respectively (Figure 2e). Group B was the FITC solution with concentrations of 0, 1, 0.5, 0.25, 0.125, 0.0625, and 0.03125 g/L, the central wavelengths of the two filters were 488 and 532 nm, respectively. And group C was the Cy5 solution with concentrations of 0, 1, 0.2, 0.04, 8×10^{-3}, 1.6×10^{-3}, and 3.2×10^{-4} g/L, the central wavelengths of the two filters were 650 and 670 nm, respectively. The fluorescence signal intensities of the solutions containing microspheres were higher than those of the corresponding solutions without microspheres in Groups A, B, and C (Figure 2e). The fluorescence signal intensity of the solution with microspheres was higher than that of the solution without microspheres at a

https://doi.org/10.1021/acsami.5c00655
ACS Appl. Mater. Interfaces XXXX, XXX, XXX−XXX

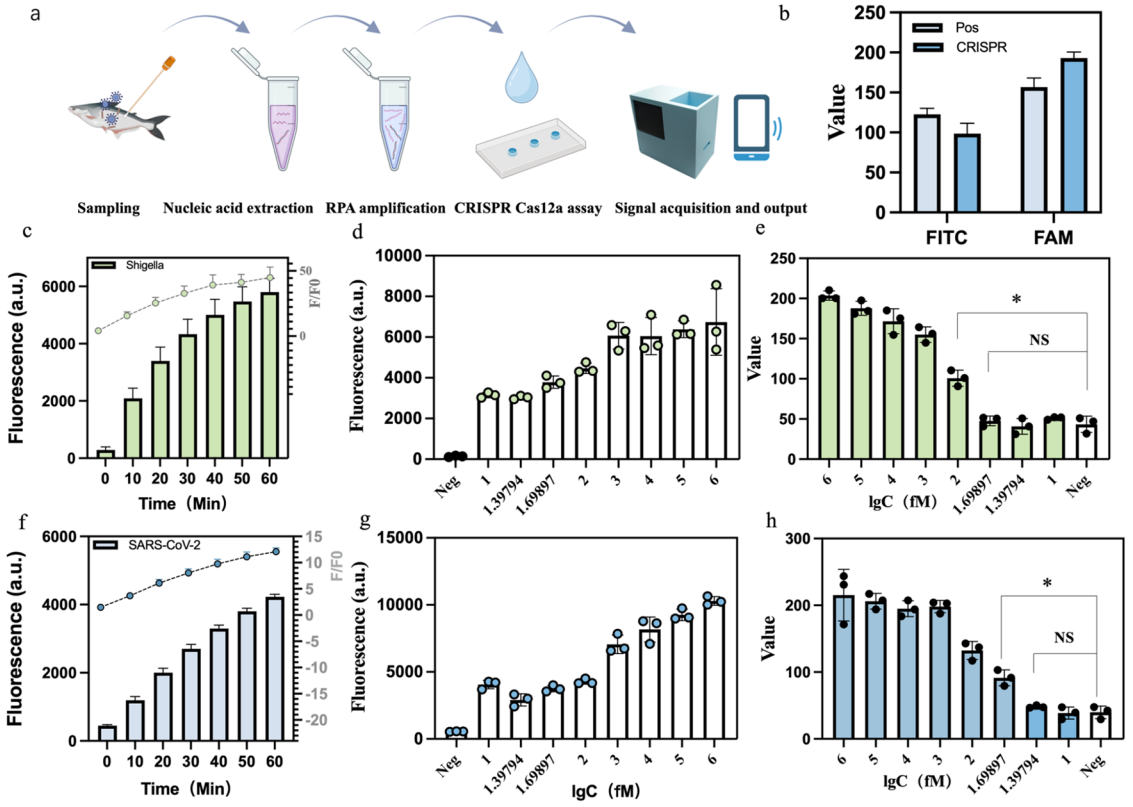


Figure 4. RPA and CRISPR-based nucleic acid detection. (a) Workflow of the detection platform in this study. (b) Comparative analysis of FITC and FAM reporters following CRISPR or MNase Assays. Data were collected by the portable device. Pos: MNase assay; CRISPR: CRISPR assay. Δ: Minus negative control. (c) The changes of fluorescence intensity by FAM reporters with *Shigella*-related Cas12a CRISPR assay time. F/F0: signal-to-background ratio. (d) The corresponding fluorescence changes of CRISPR assay to the logarithm of *Shigella* related-RPA products. Data were collected by the qPCR machine. And data were collected by the portable device shown in (e). (f) The changes of fluorescence intensity by FAM reporters with SARS-CoV-2 -related Cas12a CRISPR assay time. (g) The corresponding fluorescence changes of CRISPR assay to the logarithm of SARS-CoV-2 related-RPA products. Data were collected by the qPCR machine. And data were collected by the portable device shown in (h). *, $P < 0.05$; NS, no significance.

solution concentration of 0 g/L. This may be due to the scattering of the excitation light when passing through the microspheres, which led to the elevation of the noise signal; however, the overall signal-to-noise ratio of the microsphere chip was higher than that of the chip without microspheres. Therefore, the higher signal-to-noise enhancement at low concentrations indicates a lower LoD. As shown in Table S2, the fluorescence enhancement factors (Ratio of slope after enhancement to slope before enhancement) of the device for rhodamine 6G, FITC, and Cy5 solutions were 1.4658, 1.1945, and 1.3670, respectively. Since we used FAM as a fluorescent reporter, we used different concentrations of FAM solution to verify the enhancement effect of the microsphere system on the FAM solution, and the experimental results for Shigella and SARS-CoV-2 are shown in Figure S10a,b. The concentrations of the FAM solution used were 0, 1, 0.5, 0.25, 0.125, 0.0625, and 0.03125 g/L. The results showed that the microsphere system can effectively enhance the fluorescence signal of the FAM solution with a fluorescence enhancement factor of 1.2967. The results showed that microspheres enhanced the signals of fluorescent solutions at different wavelengths and lowered the LoD of the solutions.

3.7. RPA and Cas-Based Nucleic Acid Detection. *3.7.1. Principle of the RPA-CRISPR Method.* Nucleic acids were initially sampled and extracted from the examined specimens. Following this, RT-RPA was conducted on the isolated SARS-CoV-2 RNA, while RPA was applied to *Shigella* DNA. Next, the amplified nucleic acids were subjected to a CRISPR Cas12a reaction, which took place on a microfluidic chip. Upon detection of the target sequence, Cas12a became activated, leading to cleavage of the DNA strand between the FAM fluorophores and BHQ1, thereby generating a fluorescent signal (Figure 4a).

3.7.2. Fluorescence Reporter Screening. To identify the most effective fluorescent reporters for our POCT device, we performed micrococcal nuclease (MNase) enzymatic digestion and Cas12a cleavage experiments using FAM and FITC reporters. MNase is an endonuclease capable of directly severing the DNA strands. Upon completing the digestion experiments, the acquired data indicated that the FAM reporters demonstrated superior fluorescence intensity compared to FITC. Consistent outcomes were also observed in the Cas12a cleavage experiments. These findings suggest that FAM is a more compatible choice than FITC for the fluorescence reporting requirements of our POCT device (Figure 4b).

3.7.3. RPA-CRISPR Method with POCT Device. To ascertain the most effective duration of the Cas12a reaction at an original DNA concentration of 1 pM, we systematically gathered data at intervals of 0, 10, 20, 30, 40, 50, and 60 min using a quantitative PCR (qPCR) instrument, allowing us to evaluate the fluorescence signal development over time. The experimental data revealed that there is no significant increase

https://doi.org/10.1021/acsami.5c00655
ACS Appl. Mater. Interfaces XXXX, XXX, XXX−XXX

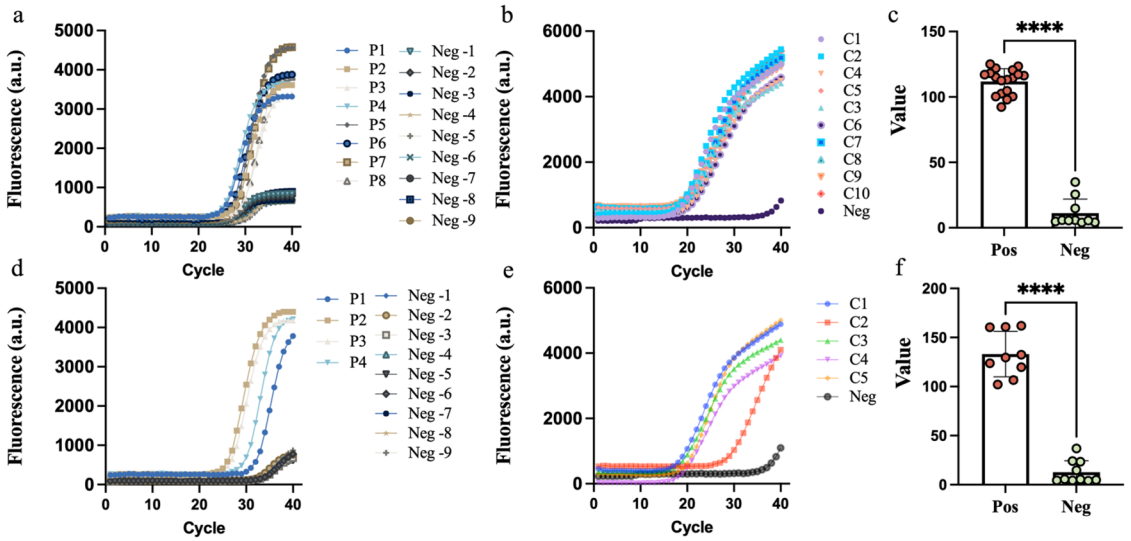


Figure 5. Feasibility of the portable device using pathogen samples. (a) qPCR detection results for SARS-CoV-2 in 8 environmental contamination samples (P1- P8) and 9 SARS-CoV-2-negative samples (2 Influenza A virus samples: Neg1−2, 2 respiratory syncytial virus samples: Neg3−4, 2 *Staphylococcus aureus* samples Neg 5−6, and 3 blank samples). (b) qPCR detection results for SARS-CoV-2 in 10 clinical samples (C1−C10) and 1 SARS-CoV-2-negative (blank sample). (c) Detection results for SARS-CoV-2 using the portable device. Red**:** Positive samples; Green: Negative samples. (d) qPCR detection results for *Shigella* in 4 food contamination samples (P1−4) and 9 *Shigella*-negative samples (4 *Escherichia coli* samples: Neg 1−4, 2 *Staphylococcus aureus* samples: Neg5−6, and 3 blank samples: Neg7−9). (e) qPCR detection results for *Shigella* in 5 clinical samples (C1−C5) and 1 SARS-CoV-2-negative (blank sample). (f) Detection results for *Shigella* using the portable device. Red: Positive samples; Green: Negative samples.

in the fluorescence intensity/background ratio after 40 min of Cas12a reaction (as shown in Figure 4c,4f). Therefore, 40 min is considered an appropriate reaction time for the CRISPR assay.

This study systematically detected target substrates from *Shigella* and SARS-CoV-2 across a concentration gradient of 1 nM to 10 fM by employing a combined CRISPR-RPA assay. The resulting fluorescence signals were meticulously analyzed using a qPCR instrument and a proprietary two POCT devices. The analytical results demonstrated that both platforms reliably produced positive signals throughout the evaluated concentration spectrum. According to the qPCR instrument data, the variability in fluorescence observed in the *Shigella* and SARS-CoV-2 RPA-Cas12a assays was proportional to the logarithm of the original concentration, as depicted in Figure 4d,g.

According to the two POCT devices, the fluorescence intensity elicited by the CRISPR assay directly correlated with the initial substrate concentration within the tested range (Figures 4e,h and S11a,b). We determined the lowest concentration that can be detected by POCT devices was considered as the LoD. We determined the LoD of *Shigella* to be 100 fM and SARS-CoV-2 to be 75 fM for devices that were photographed using a cell phone camera, while the LoD for *Shigella* was 75 fM and SARS-CoV-2 was 50 fM for devices that were photographed using a USB camera (Figures 4e,4h and S11a,b). Furthermore, the CRISPR system combined with microspheres has demonstrated superior sensitivity compared to microfluidic systems without them (*Shigella*: 250 fM vs 100 fM, Figure S12a, SARS-CoV-2:500 fM vs 75 fM, Figure S12b). This highlights the enhanced detection capabilities provided by the integration of microspheres in CRISPR-based assays. Collectively, these results substantiate the efficacy of our POCT devices for detecting SARS-CoV-2 and *Shigella* via CRISPR.

3.7.4. Validation with Pathogens Samples. In the context of our experimental validation, we procured various samples for testing SARS-CoV-2 and *Shigella* nucleic acids. For SARS-CoV-2, we obtained 10 clinical samples and 8 environmental contamination samples. Additionally, we included 2 Influenza A virus samples, 2 respiratory syncytial virus samples, 2 *Staphylococcus aureus* samples, and 4 blank samples as negative controls. Regarding *Shigella*, we procured 5 clinical samples and 4 food contamination samples from salad, containing *Shigella* nucleic acids. We also included 4 *Escherichia coli samples*, 2 *Staphylococcus aureus* samples, and 4 blank samples as negative controls.

All clinical samples, contaminated samples, and negative control samples were tested using qPCR. Specifically, SARS-CoV-2 environmental contamination samples and clinical samples were successfully detected by qPCR (Figure 5a,b). Similarly, food contamination samples and clinical samples of *Shigella* also yielded positive results in qPCR detection (Figure 5d,e). All samples were successfully detected using our POCT device using RPA and CRISPR approaches (Figure 5c,f). In both SARS-CoV-2 and *Shigella* detections, the signal values produced by the positive sample groups were significantly higher than those of the negative groups. These comparative findings underscore the ability of our POCT device to accurately identify SARS-CoV-2 and *Shigella* nucleic acids in alignment with the established protocol.

However, our technology has some limitations. First, our technology does not currently offer a markedly superior LoD compared with existing platforms, primarily because of the constraints inherent in our CRISPR-RPA detection methodology, which builds upon previous research. While our methods for detecting SARS-CoV-2 and *Shigella* are rooted in prior studies, our research introduces advancements in the form of microsphere-augmented signal enhancement for dye-reporter-based detection methods. This approach has broad

https://doi.org/10.1021/acsami.5c00655
ACS Appl. Mater. Interfaces XXXX, XXX, XXX−XXX

applicability. In this study, we evaluated commonly used dye reporters and discovered that CRISPR assays incorporating FAM reporters produced a more robust signal output within our detection system. Second, it is important to note that our test was not inclusive. Cold chain foods can be vectors for a multitude of potential pathogens, and our focus on SARS-CoV-2 and *Shigella* represents only a small fraction of the possible pathogens. Due to sample limitations, we were unable to conduct feasibility tests using abundant samples.

4. CONCLUSIONS

Foodborne contamination during cold chain transportation poses significant risks to public health. Therefore, it is imperative to have rapid, accurate, timely, and immediate detection methods in place to control the spread of infection and safeguard public well-being. RPA and CRISPR assays provide the benefit of constant-temperature operation, paired with the design of a compact, lightweight analysis device, which helps to overcome the limitations of large and intricate qPCR machines. Furthermore, these methods boast the benefits of specificity and rapidity. Meanwhile, the microsphere-based optofluidic system offers a straightforward and cost-effective approach to boosting fluorescence signal intensity. In our research, we have combined a microsphere-enhanced optofluidic system with RPA and CRISPR technologies to create a method for nucleic acid detection that is rapid, accurate, and sensitive. The method's effectiveness was confirmed through the analysis of clinical and contamination samples. The experimental results show that the LoD of *Shigella* and SARS-CoV-2 are 100 fM (POCT with USB camera: 75 fM) and 75 fM (POCT with USB camera: 50 fM), respectively. The total detection time of the device is approximately 50 min. Compared with traditional detection methods, this system has the advantages of small size, easy operation, low detection cost, and portability.

However, the potential applications of this platform extend far beyond this. The platform is flexible enough to adapt to the detection requirements of various settings, i.e., it is also suitable for pathogen detection in community hospitals and resource-limited areas. Notably, this technique possesses broad applicability, allowing for the detection of nucleic acids from various pathogens by merely adjusting the sequences that RPA and CRISPR target. Nevertheless, the device has certain drawbacks. For instance, compared with previous POCT-related studies, this study does not show a significant advantage in terms of detection limit. Specifically, our detection limit is similar to that reported in previous studies on POCT and shows a slight improvement compared to the detection limits observed in other comparable investigations.[33−35] And it does not facilitate the concurrent detection of multiple pathogens within a single sample. In the subsequent research, we envision the simultaneous excitation of multiple DNA/RNA reporters combining Cas12 and Cas 13 in the same sample by deploying multiple lasers and adjusting the optical path system to allow simultaneous access to the sample to be tested. This optofluidic system can be further improved using multiple filters and CCD device signal-receiving modules to simultaneously receive fluorescent signals of different wavelengths emitted from the same sample and develop corresponding image-processing algorithms for detection and analysis, thus realizing the simultaneous detection of different accounting samples. We believe that this optofluidic platform will benefit communities, remote areas, and patients.

■ ASSOCIATED CONTENT

Data Availability Statement

All data required to evaluate the conclusions are presented in the manuscript and/or Supporting Information. Additional data related to this paper may be requested from the authors.

Supporting Information

The Supporting Information is available free of charge at https://pubs.acs.org/doi/10.1021/acsami.5c00655.

Supplementary experimental details, nucleotide sequence, and figures (PDF)

■ AUTHOR INFORMATION

Corresponding Authors

Yuan Rong − *Department of Laboratory Medicine, Center for Single-Cell Omics and Tumor Liquid Biopsy, Zhongnan Hospital of Wuhan University, Wuhan 430071, China*; Email: rongyuan323@whu.edu.cn

Yi Yang − *School of Physics & Technology, Department of Clinical Laboratory, Institute of Medicine and Physics, Zhongnan Hospital, Renmin Hospital, Wuhan University, Wuhan 430072, China; Shenzhen Research Institute, Wuhan University, Shenzhen 518000, China*; orcid.org/0000-0003-0693-9193; Email: yangyiys@whu.edu.cn

Fubing Wang − *Department of Laboratory Medicine, Center for Single-Cell Omics and Tumor Liquid Biopsy, Zhongnan Hospital of Wuhan University, Wuhan 430071, China*; orcid.org/0000-0002-5971-2622; Email: wangfubing@znhospital.cn

Chunhui Yuan − *Department of Laboratory Medicine, Wuhan Children's Hospital (Wuhan Maternal and Child Healthcare Hospital), Tongji Medical College, Huazhong University of Science and Technology, Wuhan 430015, China*; Email: chunhuii.yuen@whu.edu.cn

Authors

Menglu Gao − *Department of Laboratory Medicine, Center for Single-Cell Omics and Tumor Liquid Biopsy, Zhongnan Hospital of Wuhan University, Wuhan 430071, China*

Chen Yang − *School of Physics & Technology, Department of Clinical Laboratory, Institute of Medicine and Physics, Zhongnan Hospital, Renmin Hospital, Wuhan University, Wuhan 430072, China; Shenzhen Research Institute, Wuhan University, Shenzhen 518000, China*

Wu Si − *Department of Laboratory Medicine, Center for Single-Cell Omics and Tumor Liquid Biopsy, Zhongnan Hospital of Wuhan University, Wuhan 430071, China*

Xiaodan Xi − *Department of Laboratory Medicine, Center for Single-Cell Omics and Tumor Liquid Biopsy, Zhongnan Hospital of Wuhan University, Wuhan 430071, China*

Liangjun Chen − *Department of Laboratory Medicine, Center for Single-Cell Omics and Tumor Liquid Biopsy, Zhongnan Hospital of Wuhan University, Wuhan 430071, China*

Zhikun Zeng − *Department of Laboratory Medicine, Center for Single-Cell Omics and Tumor Liquid Biopsy, Zhongnan Hospital of Wuhan University, Wuhan 430071, China*

Complete contact information is available at: https://pubs.acs.org/10.1021/acsami.5c00655

https://doi.org/10.1021/acsami.5c00655
ACS Appl. Mater. Interfaces XXXX, XXX, XXX−XXX

Author Contributions

[⊥]G.M., C.Y., S.W., and X.X. contributed equally to this paper. The manuscript was collaboratively authored by all contributors, who have all endorsed the final draft.

Funding

This work was funded by the Translational Medicine and Interdisciplinary Research Joint Fund of Zhongnan Hospital of Wuhan University (ZNJC202002), Key technology development and application of novel coronavirus detection in cold chain food and related environment (2021ACB002), National Natural Science Foundation of China (No. 62175190), and Guangdong Basic and Applied Basic Research Foundation (No. 2024A1515012104).

Notes

The authors declare no competing financial interest.

■ ACKNOWLEDGMENTS

We would like to express our gratitude to the Department of Laboratory Medicine, Center for Single-Cell Omics and Tumor Liquid Biopsy at Zhongnan Hospital of Wuhan University for their outstanding technical assistance and support with sample provision.

■ ABBREVIATIONS

CRISPR:clustered regularly interspaced short palindromic repeats
Cy5:cyanine5
FAM:fluorescein amidite
FITC:fluorescein isothiocyanate
LoD:limit of detection
MNase:micrococcal nuclease
PCR:polymerase chain reaction
PDMS:polydimethylsiloxane
POCT:point-of-care testing
PS:Polystyrene
R6G:Rhodamine 6G
RPA:recombinase polymerase amplification
RT-qPCR:reverse transcription quantitative PCR

■ REFERENCES

(1) Kumar, P.; Meghvansi, M. K.; Kamboj, D. V. Isolation, phenotypic characterization and comparative genomic analysis of 2019SD1, a polyvalent enterobacteria phage. *Sci. Rep.* **2021**, *11* (1), No. 22197.

(2) Phalipon, A.; Sansonetti, P. J. Shigella's ways of manipulating the host intestinal innate and adaptive immune system: a tool box for survival? *Immunol. Cell Biol.* **2007**, *85* (2), 119−129.

(3) Park, S. M.; Choi, C.; Rhee, M. S. One Health approach for prioritization of potential foodborne pathogens: Risk-ranking, Delphi survey, and criteria evaluation pre- and post-COVID-19 pandemic. *Compr Rev. Food Sci. Food Safe* **2024**, *23* (1), No. e13258.

(4) Maragoni-Santos, C.; Serrano Pinheiro de Souza, T.; Matheus, J. R. V.; de Brito Nogueira, T. B.; Xavier-Santos, D.; Miyahira, R. F.; Costa Antunes, A. E.; Fai, A. E. C. COVID-19 pandemic sheds light on the importance of food safety practices: risks, global recommendations, and perspectives. *Crit Rev. Food Sci. Nutr.* **2022**, *62* (20), 5569−5581.

(5) Tian, Z.; Yan, H.; Zeng, Y. Solid-Phase Extraction and Enhanced Amplification-Free Detection of Pathogens Integrated by Multifunctional CRISPR-Cas12a. *ACS Appl. Mater. Interfaces* **2024**, *16* (12), 14445−14456.

(6) Zai, Y.; Min, C.; Wang, Z.; Ding, Y.; Zhao, H.; Su, E.; He, N. A sample-to-answer, quantitative real-time PCR system with low-cost, gravity-driven microfluidic cartridge for rapid detection of SARS-CoV-2, influenza A/B, and human papillomavirus 16/18. *Lab Chip* **2022**, *22* (18), 3436−3452.

(7) Saiki, R. K.; Gelfand, D. H.; Stoffel, S.; Scharf, S. J.; Higuchi, R.; Horn, G. T.; Mullis, K. B.; Erlich, H. A. Primer-Directed Enzymatic Amplification of DNA with a Thermostable DNA Polymerase. *Science* **1988**, *239* (4839), 487−491.

(8) Zhu, H. L.; Zhang, H. Q.; Ni, S.; Korabecná, M.; Yobas, L.; Neuzil, P. The vision of point-of-care PCR tests for the COVID-19 pandemic and beyond. *TrAc-Trend Anal. Chem.* **2020**, *130*115984.

(9) Hao, L.; Zhao, R. T.; Welch, N. L.; Tan, E. K. W.; Zhong, Q.; Harzallah, N. S.; Ngambenjawong, C.; Ko, H.; Fleming, H. E.; Sabeti, P. C.; Bhatia, S. N. CRISPR-Cas-amplified urinary biomarkers for multiplexed and portable cancer diagnostics. *Nat. Nanotechnol.* **2023**, *18* (7), 798−807.

(10) Samanta, D.; Ebrahimi, S. B.; Ramani, N.; Mirkin, C. A. Enhancing CRISPR-Cas-Mediated Detection of Nucleic Acid and Non-nucleic Acid Targets Using Enzyme-Labeled Reporters. *J. Am. Chem. Soc.* **2022**, *144* (36), 16310−16315.

(11) Yin, L.; Man, S.; Ye, S.; Liu, G.; Ma, L. CRISPR-Cas based virus detection: Recent advances and perspectives. *Biosens. Bioelectron.* **2021**, *193*, No. 113541.

(12) Jiao, C.; Peeck, N. L.; Yu, J.; Ghaem Maghami, M.; Kono, S.; Collias, D.; Martinez Diaz, S. L.; Larose, R.; Beisel, C. L. TracrRNA reprogramming enables direct PAM-independent detection of RNA with diverse DNA-targeting Cas12 nucleases. *Nat. Commun.* **2024**, *15* (1), No. 5909.

(13) Wu, L.; Wang, X.; Wu, X.; Xu, S.; Liu, M.; Cao, X.; Tang, T.; Huang, X.; Huang, H. MnO(2) Nanozyme-Mediated CRISPR-Cas12a System for the Detection of SARS-CoV-2. *ACS Appl. Mater. Interfaces* **2022**, *14* (45), 50534−50542.

(14) Fozouni, P.; Son, S.; Díaz de León Derby, M.; Knott, G. J.; Gray, C. N.; D'Ambrosio, M. V.; Zhao, C.; Switz, N. A.; Kumar, G. R.; Stephens, S. I.; et al. Amplification-free detection of SARS-CoV-2 with CRISPR-Cas13a and mobile phone microscopy. *Cell* **2021**, *184* (2), 323−333.e329.

(15) Ganguli, A.; Mostafa, A.; Berger, J.; Aydin, M. Y.; Sun, F.; Ramirez, S. A. S. d.; Valera, E.; Cunningham, B. T.; King, W. P.; Bashir, R. Rapid isothermal amplification and portable detection system for SARS-CoV-2. *Proc. Natl. Acad. Sci. U.S.A.* **2020**, *117* (37), 22727−22735.

(16) Cheong, J.; Yu, H.; Lee, C. Y.; Lee, J.-u.; Choi, H.-J.; Lee, J.-H.; Lee, H.; Cheon, J. Fast detection of SARS-CoV-2 RNA via the integration of plasmonic thermocycling and fluorescence detection in a portable device. *Nature Biomedical Engineering* **2020**, *4* (12), 1159−1167.

(17) Li, Z.; Zhang, S.; Zhang, J.; Avery, L.; Banach, D.; Zhao, H.; Liu, C. Palm-Sized Lab-In-A-Magnetofluidic Tube Platform for Rapid and Sensitive Virus Detection. *Adv. Sci.* **2024**, *11* (23), No. e2310066.

(18) Chen, L.; Yu, L.; Liu, Y.; Xu, H.; Ma, L.; Tian, P.; Zhu, J.; Wang, F.; Yi, K.; Xiao, H.; et al. Space-time-regulated imaging analyzer for smart coagulation diagnosis. *Cell Rep. Med.* **2022**, *3* (10), No. 100765.

(19) Chen, L.; Yu, L.; Chen, M.; Liu, Y.; Xu, H.; Wang, F.; Zhu, J.; Tian, P.; Yi, K.; Zhang, Q.; et al. A microfluidic hemostatic diagnostics platform: Harnessing coagulation-induced adaptive-bubble behavioral perception. *Cell Rep. Med.* **2023**, *4* (11), No. 101252.

(20) Cai, Q. W.; Ju, X. J.; Zhang, S. Y.; Chen, Z. H.; Hu, J. Q.; Zhang, L. P.; Xie, R.; Wang, W.; Liu, Z.; Chu, L. Y. Controllable Fabrication of Functional Microhelices with Droplet Microfluidics. *ACS Appl. Mater. Interfaces* **2019**, *11* (49), 46241−46250.

(21) Chen, J.; Spoljaric, S.; Calatayud-Sanchez, A.; Alvarez-Brana, Y.; Caruso, F. Engineering Metal-Phenolic Network Nanoparticles via Microfluidics. *ACS Appl. Mater. Interfaces* **2023**, *15* (41), 48050−48059.

(22) Hu, X.; Zheng, J.; Zhu, Q.; Wu, Q.; Li, S.-S.; Yang, Y.; Chen, L.-J. Acoustic Assembly and Scanning of Superlens Arrays for High-Resolution and Large Field-of-View Bioimaging. *ACS Nano* **2024**, *18* (23), 15218−15228.

https://doi.org/10.1021/acsami.5c00655
ACS Appl. Mater. Interfaces XXXX, XXX, XXX−XXX

(23) Zhu, J.; Han, G.; Hu, X.; Zuo, Y.; Chen, L.; Wang, F.; Yang, Y.; Jiang, F.; Sun, C.; Zhao, W.; Han, X. A Portable and Accurate Phosphate Sensor Using a Gradient Fabry−Pérot Array. *ACS Sens.* **2020**, *5* (5), 1381−1388.
(24) He, G.; Zhao, S.; Yang, C.; Chen, L.; Liu, Y.; Hu, Q.; Yang, Y. Point-of-care monitoring of milk quality by rapid Immunofluorescence with mechanical deformation of the hydrogel microspheres. *Sens. Actuators, B* **2024**, *417*, No. 136160.
(25) Yang, C.; He, G.; Liu, Y.; Ma, Y.; Jiang, T.; Gao, X.; Zhao, S.; Chen, L.; Zhang, X.; Yi, K.; et al. Accurate point-of-care lotus biomimetic microfluidic urine testing platform for patients with chronic kidney disease. *Chem. Eng. J.* **2024**, *497*, No. 154736.
(26) Goncharov, A.; Joung, H. A.; Ghosh, R.; Han, G. R.; Ballard, Z. S.; Maloney, Q.; Bell, A.; Aung, C. T. Z.; Garner, O. B.; Carlo, D. D.; Ozcan, A. Deep Learning-Enabled Multiplexed Point-of-Care Sensor using a Paper-Based Fluorescence Vertical Flow Assay. *Small* **2023**, *19* (51), No. e2300617.
(27) Liu, J.; Li, N.; Zhang, L.; Lu, Y.; Shen, M.; Zhang, Y.; Feng, L.; Jing, J.; Cheng, J.; Xu, Y. A Wax Interface-Enabled One-Pot Multiplexed Nucleic Acid Testing Platform for Rapid and Sensitive Detection of Viruses and Variants. *Small Methods* **2024**, *8* (8), No. e2400030.
(28) Yi, J.; Gao, Z.; Guo, Q.; Wu, Y.; Sun, T.; Wang, Y.; Zhou, H.; Gu, H.; Zhao, J.; Xu, H. Multiplexed digital ELISA in picoliter droplets based on enzyme signal amplification block and precisely decoding strategy: A universal and practical biodetection platform. *Sens. Actuators, B* **2022**, *369*, No. 132214.
(29) Zeng, H.; Katagiri, D.; Ogino, T.; Nakajima, H.; Kato, S.; Uchiyama, K. Droplet Enhanced Fluorescence for Ultrasensitive Detection Using Inkjet. *Anal. Chem.* **2016**, *88* (12), 6135−6139.
(30) Kaneko, T.; Sun, Y.; Nakajima, H.; Uchiyama, K.; Zeng, H. Droplet Sensitized Fluorescence Detection for Enzyme-Linked Immune Sorbent Assays on Microwell Plate. *Anal. Chem.* **2019**, *91* (9), 5685−5689.
(31) Jana, S.; Xu, X.; Klymchenko, A.; Reisch, A.; Pons, T. Microcavity-Enhanced Fluorescence Energy Transfer from Quantum Dot Excited Whispering Gallery Modes to Acceptor Dye Nanoparticles. *ACS Nano* **2021**, *15* (1), 1445−1453.
(32) Broughton, J. P.; Deng, X.; Yu, G.; Fasching, C. L.; Servellita, V.; Singh, J.; Miao, X.; Streithorst, J. A.; Granados, A.; Sotomayor-Gonzalez, A.; et al. CRISPR-Cas12-based detection of SARS-CoV-2. *Nat. Biotechnol.* **2020**, *38* (7), 870−874.
(33) Shi, Y.; Kang, L.; Mu, R.; Xu, M.; Duan, X.; Li, Y.; Yang, C.; Ding, J. W.; Wang, Q.; Li, S. CRISPR/Cas12a-Enhanced Loop-Mediated Isothermal Amplification for the Visual Detection of Shigella flexneri. *Front. Bioeng. Biotechnol.* **2022**, *10*, No. 845688.
(34) Liu, S.; Xie, T.; Huang, Z.; Pei, X.; Li, S.; He, Y.; Tong, Y.; Liu, G. Systematically investigating the fluorescent signal readout of CRISPR-Cas12a for highly sensitive SARS-CoV-2 detection. *Sens. Actuators, B* **2022**, *373*, No. 132746.
(35) Curtin, K.; Wang, J.; Fike, B. J.; Binkley, B.; Li, P. A 3D printed microfluidic device for scalable multiplexed CRISPR-cas12a biosensing. *Biomed. Microdevices* **2023**, *25* (3), 34.

https://doi.org/10.1021/acsami.5c00655
ACS Appl. Mater. Interfaces XXXX, XXX, XXX−XXX